The stability of self-organized 1-nonanethiol-capped gold nanoparticle monolayer

2001 J. Phys. D: Appl. Phys. 34 2255

(http://iopscience.iop.org/0022-3727/34/15/303)

INSTITUTE OF PHYSICS PUBLISHING JOURNAL OF PHYSICS D: APPLIED PHYSICS
J. Phys. D: Appl. Phys. **34** (2001) 2255–2259 PII: S0022-3727(01)23004-6

The stability of self-organized 1-nonanethiol-capped gold nanoparticle monolayer

Peng Jiang[1], Si-shen Xie[1], Jian-nian Yao[2], Shi-jin Pang[1] and Hong-jun Gao[1]

[1] Beijing Laboratory of Vacuum Physics, Institute of Physics and Center for Condensed Matter Physics, Chinese Academy of Sciences, PO Box 2724, Beijing 100080, People's Republic of China
[2] Center for Molecular Sciences, Institute of Chemistry, Chinese Academy of Sciences, Beijing 100101, People's Republic of China

Received 19 March 2001, in final form 6 June 2001
Published 17 July 2001
Online at stacks.iop.org/JPhysD/34/2255

Abstract
1-Nonanethiol-protected gold nanoparticles with the size of about 2 nm have been prepared by a wet chemical method through choosing a suitable ratio of Au:S (2.5:1). Size selective precipitation of nanoparticles has been used to narrow their size distribution, which facilitates the formation of an ordered nanoparticle close-packed structure. A Fourier transform infrared investigation provides the evidence of the encapsulation of Au nanoparticles by 1-nonanethiol while an ultraviolet–visible spectrum shows a broad absorption around 520 nm, corresponding to surface plasmon band of Au nanoparticles. X-ray photoelectron spectroscopy of the samples demonstrates the metallic state of the gold (Au^0) and the existence of sulfur (S). The data from x-ray powder diffraction measurements confirm that the gold nanoparticles have the same face-centred cubic crystalline structure as the bulk gold phase. Finally, transmission electron microscopy (TEM) characterization indicates that the size of the monodisperse colloidal gold nanoparticles is about 2 nm and they can self-organize to form a two-dimensional hexagonal close-packed structure after evaporating a concentrated drop of nanoparticles–toluene solution on a carbon-coated TEM copper grid.

1. Introduction

The realization of an ordered arrangement of noble metallic or semiconductor nanoparticles has been the main objective for the application of mesoscopic systems in macroscopic devices [1]. One strategy is how to prepare monodisperse nanoparticles and use them as 'building blocks' to construct mesoscopic ordered architectures. Among the techniques being investigated, a simple and effective method is a wet colloidal chemical synthesis technique, which allows one to conveniently control the size and distribution of the nanoparticles. The metallic nanoparticles obtained by the method typically consist of a metal core and capped ligands which are employed as stabilizers to dominate the nucleation and growth of the nanoparticles in a solvent or as functionalized molecules to react with other compounds [2–6]. Brust *et al* [7] first showed that alkylthiol-passivated Au nanoparticles with the size of 2 ± 1 nm could be synthesized using the above approach in a two-phase aqueous/organic system. Later, Leff *et al* [8] further reported that the diameter of the Au nanoparticles could be determined exclusively by the initial $AuCl_4^-$:thiol ratio. Provided the size distribution is narrow enough and experimental conditions are optimized, the sterically stabilized nanoparticles can self-organize into two-dimensional (2D) [9] or three-dimensional (3D) superlattice structures [10]. Recently, Martin *et al* [11] investigated the formation of 2D and 3D superlattices of Au nanoparticles synthesized in non-ionic inverse micelles. They employed variable chain length thiols from C_6 to C_{18} as ligands and found that intermediate alkanethiols, from C_6SH to $C_{14}SH$,

easily resulted in the formation of uniform superlattices with controlled gaps. However, up to now, although a substantial number of investigations in the formation of such superlattices have been reported, most similar studies involved only even carbon chain thiols, little work has focused on odd carbon chains as ligands. In this paper, we utilized 1-nonanethiol molecules as stabilizers in order to prepare Au nanoparticles of about 2 nm in diameter through choosing a suitable ratio of Au:S (2.5:1). Size selected precipitation was employed to narrow the distribution of the nanoparticles. Various techniques including infrared (IR), ultraviolet–visible (UV–vis), x-ray photoelectron spectroscopy (XPS), and x-ray powder diffraction (XRD) were used to characterize the thiol-capped colloidal Au nanoparticles. When depositing a drop of the Au colloidal nanoparticle–toluene solution on carbon-coated transmission electron microscopy (TEM) copper grid, we found the formation of an ordered colloidal gold nanoparticle monolayer film. Furthermore, the stability of the ordered structure was investigated by TEM.

2. Experimental section

2.1. Materials

$HAuCl_4 \cdot 3H_2O$ (Acros, 99.8%), tetra-n-octylammonium bromide (Acros, 98%), $NaBH_4$ (Acros, 99%), 1-nonanethiol ($C_9H_{19}SH$) (Aldrich, 99%) were used as received. AR grade solvents and deionized and subsequently distilled water were used.

2.2. Synthesis and purification

Colloidal gold nanoparticles were synthesized using the method given in [7] and described as follows. First, 0.1 M tetra-n-octylammonium bromide toluene solution (10 ml) was added into a vigorously stirred 0.03 M $HAuCl_4 \cdot 3H_2O$ aqueous solution (15 ml). After stirring for 10 min, the orange/red organic phase (upper layer) was collected and the water phase was removed. Then, 0.18 mmol 1-nonanethiol was injected into the organic solution, followed by the addition of 0.4 M sodium borohydride aqueous solution (12 ml) drop by drop. After the reaction mixture was successively stirred for 24 h, the deep brown organic phase was separated from the aqueous phase and concentrated to about 5 ml by decompression distillation. After that, methanol (200 ml) was poured into the residual dispersion to effectively precipitate the gold nanoparticles. The black precipitate was collected by filtering the mixture with a 2.5 μm polypropylene filter paper and washed repeatedly several times with ethanol, to remove excess surfactants. Size selective precipitation employing chloroform and methanol as solvents was used to narrow the size distribution of the product. The black precipitate was dissolved in 10 ml chloroform, then 100 ml methanol was added to precipitate gold nanoparticles continuously. The precipitates were collected every 4 h, sometimes pure water was dripped into the solution to accelerate the precipitation process. The product collected in the middle of each 4 h period was retained. Finally, the thus-obtained nearly monodisperse 2 nm sized gold nanoparticles were prepared for various characterizations.

2.3. Spectroscopic studies

Fourier transform infrared (FT–IR) spectra were recorded on a Bio-Rad FT-IR spectrophotometer using a 150 mg KBr disc dispersed with the colloidal gold–toluene solution or a drop of 1-nonanethiol liquid. Background correction was performed using a reference blank KBr pellet. UV–vis absorption spectra of the colloidal gold nanoparticle dispersion in cyclohexane were measured using a Shimadzu UV-1601 PC double-beam spectrophotometer in the range 200–800 nm with 2 nm resolution.

2.4. XRD

XRD was performed on a Rigaku D/MAX2000 x-ray diffractometer with Cu Kα ($\lambda = 1.5418$ Å) radiation operating at 40 kV and 20 mA. The diameter of the gold nanoparticles was estimated in terms of the broadening of the width at half-height of the first diffraction peak by employing Scherrer's equation.

2.5. XPS

XPS of the gold nanoparticles were obtained on a VG ESCALAB 5 Multi-technique Electron Spectrum Meter that focused monochromatic Al Kα x-rays onto the sample.

2.6. TEM

The TEM experiments were performed by depositing a drop of a toluene solution of the colloidal gold nanoparticles onto a carbon-coated copper grid and letting it dry completely under ambient conditions. Transmission electron micrographs were obtained from a Hitachi-800 TEM system operating at 200 kV.

3. Results and discussion

3.1. IR spectral characterization

Fourier transform infrared spectra (FT-IR) of pure 1-nonanethiol molecules and the thiol-capped gold nanoparticles are shown as curves a and b in figure 1. For clarity, the high- and low-frequency regions (see figures 1(A) and 1(B)) are given separately. The comparison of the FT-IR spectra reveals similar features in the wavelength range from 3000 to 500 cm^{-1}, strongly suggesting that 1-nonanethiol has indeed been an essential component of the composite. A further observation of a and b in figure 1(A) demonstrates that the bands assigned to the C–H asymmetric and symmetric methylene stretching vibration are shifted to lower wavenumbers in the nanocrystal spectrum, $\nu_{as}(CH_2)$ shifts from 2927 to 2921 cm^{-1} and $\nu_s(CH_2)$ shifts from 2855 to 2851 cm^{-1}, implying that the methylene vibrations of the 1-nonanethiol molecule have been confined due to the formation of relatively close-packed 3D alkanethiol self-assembled monolayers (SAMs) on the gold nanoparticle surfaces. However, the shifts of the methylene bands are slightly smaller than those corresponding of SAMs assembled on planar gold substrates ($\Delta\nu_{as}(CH_2) \approx 10$ cm^{-1} and $\Delta\nu_s(CH_2) \approx 5$ cm^{-1}). At the same time, it can be easily seen from figure 1(A) that those vibration modes corresponding

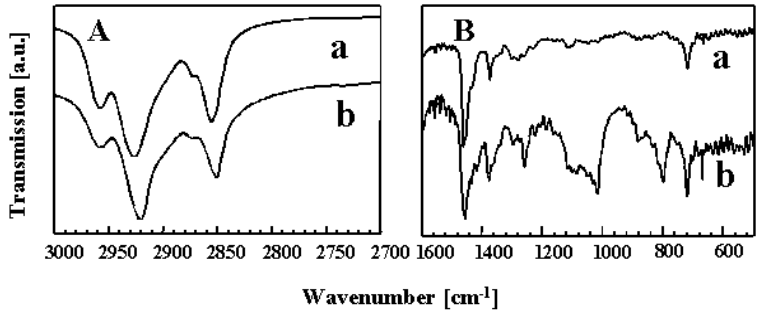

Figure 1. FT-IR spectra in the regions of high- (A) and low-frequency (B) for free 1-nonanethiol (curve a) and 1-nonanethiol-capped Au nanoparticles (curve b) on KBr window.

to the asymmetric in-plane ($\nu_{as}(CH_3) = 2928\ cm^{-1}$) and symmetric stretching ($\nu_s(CH_3) = 2871\ cm^{-1}$) vibration of the terminal methyl group seem to remain invariant with respect to capping. All of these results indicate that the 3D SAMs are less close-packed than the SAMs assembled on flat gold substrates. The methyl group at the alkane-chain terminal keeps considerable oriented freedom, which may be attributed to the extreme curvature of the nanocrystal surfaces, leading to an increase of the intermolecular space with radial distance.

In figure 1(B), a remarkable character is that the intensities of various bands are increased to some extent in the region between 1600 and 500 cm^{-1} in the nanocrystal spectrum. With deeper analysis, we find that the band assigned to C–C stretching vibrations in the broad region from 1200 to 800 cm^{-1} becomes far stronger compared to the pure 1-nonanethiol. The intensities of the bending vibrations of the terminal methyl group at 1460 ($\delta_{as}(CH_3)$) and 1379 cm^{-1} ($\delta_s(CH_3)$) are found to increase 40 and 20%, respectively. In addition, the bands involved in the C–H rocking (720 cm^{-1}), twisting and wagging (1350–1180 cm^{-1}) vibrations of the methylene group are also dramatically enhanced due to the encapsulation effect. Up to now, the phenomena have not been precisely explained. A possible qualitative explanation originates from the special orientation of the alkanethiol molecules adsorbed on the gold nanoparticle surfaces.

3.2. Uv–vis spectroscopy

An optical absorption spectrum of 1-nonanethiol-capped gold nanoparticles in cyclohexane is shown in figure 2, curve a. For comparison, we also provide the extinction spectrum of 5 nm gold nanoparticles with the same stabilizer in cyclohexane (see figure 2, curve b). A continuously increasing background towards shorter wavelengths, resulting from the Mie scattering of the suspension, can be observed for the two samples. In the case of 5 nm particles, a clear peak maximum corresponding to the plasmon excitation occurs around 520 nm, but for the gold nanoparticles synthesized in the experiment only a broad surface plasmon band superimposed on the background around 520 nm appears. This result agrees with that reported by Alzarez *et al* [12], which shows that the plasmon band cannot be intrinsically distinguished for the gold nanoparticles with an effective diameter of less than 2.0 nm.

Another important piece of information can be obtained from the peak width, which is related to the free electron collision time. It can be seen from figure 2 that the peak

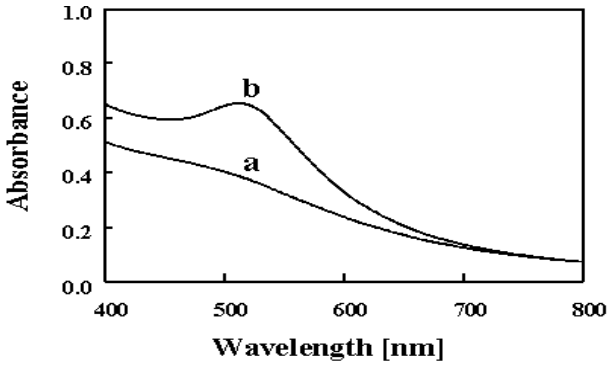

Figure 2. UV–vis spectra of the synthesized 2 nm gold nanoparticles (curve a) and the corresponding 5 nm gold nanoparticles (curve b) in cyclohexane.

width in curve a is larger than that in curve b. This means that the electron motion within nanoparticles is confined more and more as the particle size decreases. As a result, the collision time between electrons is decreased. This is a probable reason for the increase of the peak width.

3.3. XPS

The XPS spectra can provide us with information on the presence of Au and S in the nanoparticles. Figure 3 shows the scanning range from 80 to 95 eV for the gold nanoparticle sample, in which a double-peak occurs at 83.7 and 87.3 eV, corresponding to $Au_{4f7/2}$ and $Au_{4f5/2}$ respectively. This is typical for the presence of the Au^0 state. Moreover, it is worth noting that we do not find the obvious peak of the Au I state at 84.9 eV for the Au I octanethiolate complex, presumably suggesting that the interaction between Au and S is likely to be less strong than the conventional Au–S chemical bond. In addition, the sulfur region (not shown here) exhibits weaker broad double peaks at 163.1 and 162.1 eV, showing the existence of S on the surfaces of the gold nanoparticles.

3.4. The studies of inner crystal structure of nanoparticles

Figure 4 gives XRD patterns of Au films evaporated on a glass substrate (figure 4, curve a) and 1-nonanethiol-capped gold nanoparticles (figure 4, curve b). In figure 4, curve b, it appears that all of the peaks are broadened. Their shape and intensities result from diffraction from the finite number of atomic planes,

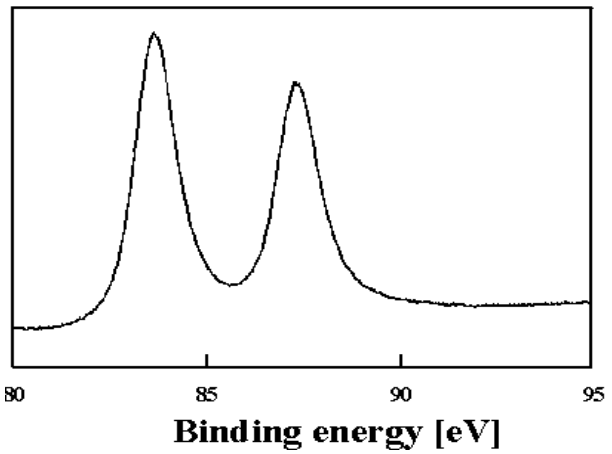

Figure 3. Partial XPS spectrum of the gold nanoparticles showing double peaks with the binding energies of 83.9 and 87.7 eV corresponding $Au4f_{7/2}$ and $Au4f_{5/2}$, respectively.

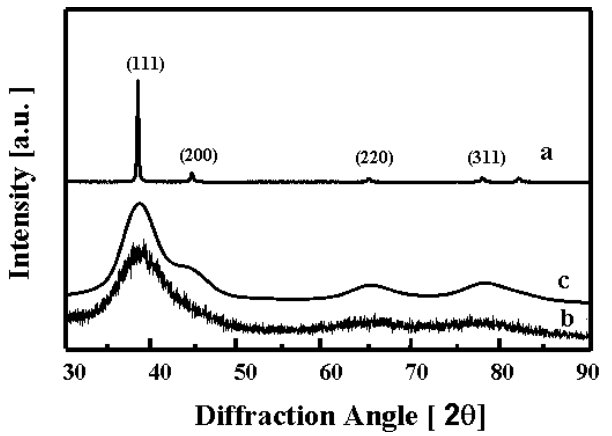

Figure 4. XRD patterns of a gold film evaporated on glass substrate (curve a) and gold nanoparticles (curve b). The calculated pattern for an untwinned 2.0 nm (Au_{314}) crystallite is shown on curve c.

attributed to the characteristic of the face-centred cubic (fcc) Au crystal structure. For clarity, we also show the calculated pattern for an untwinned Au crystallite (see figure 4, curve c), which fits well the experimental result, suggesting that the gold nanoparticles have the same crystal structure as the bulk gold. A further contrast of curves a and b in figure 4 demonstrates that all peaks become indistinct for the small nanoparticles except ⟨111⟩ and ⟨200⟩. As reported by other groups, the size of the nanoparticles can be roughly estimated using Scherrer's equation [13] according to the broading of the ⟨111⟩ peak (1.8 nm), which is very consistent with that measured by TEM as is described in the following.

3.5. The stability of the superlattice structure

TEM can provide valuable information on the size and the polydispersity of the alkanethiol-capped gold nanocrystals. Chen *et al* [14] combined TEM with differential pulse voltammetry to present the relationship between quantized double-layer charging peaks and the core size of the alkanethiol-capped gold nanocrystals. In our experiments, TEM is mainly used to characterize the polydispersity of

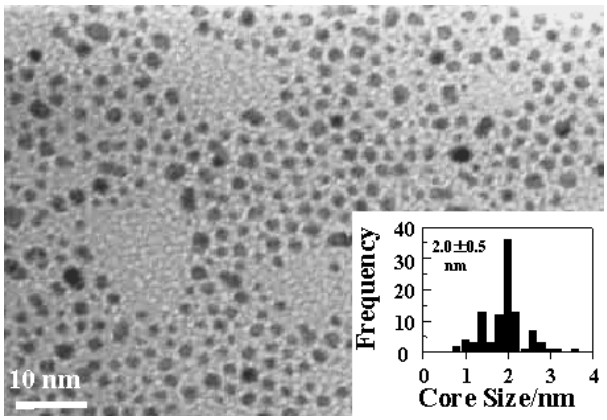

Figure 5. TEM image of the 1-nonanethiol-capped gold nanoparticles before the size distribution was narrowed. The inset shows the size distribution.

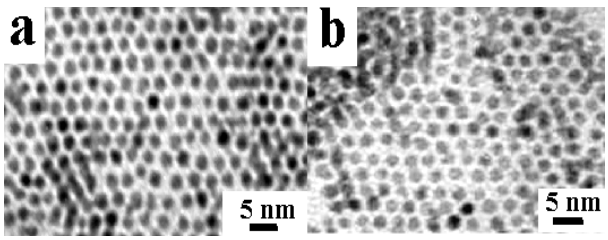

Figure 6. TEM images of the 2D ordered hexagonal-close-packed structure consisting of 1-nonanethiol-capped gold nanoparticles (a) after the size distribution was narrowed and (b) irradiated by an electron beam for 1 s.

the synthesized gold nanoparticles and the stability of the 2D nanoparticle superlattice structure. Figure 5 shows a typical TEM image and a corresponding histogram of the gold nanoparticles on a carbon-coated copper grid, which gives an average diameter of 2.0 ± 0.5 nm. Obviously, a long-range-ordered arrangement of the nanocrystals is not observed in this image due to the broad size distribution. However, further analysis reveals that the tendency of the size selective crystallization and phase separation seems to emerge, which is attributed to the effect of the size dependence of the dispersional interactions. Meanwhile, the tendency implies that reversible crystallization can occur when the system is sufficiently mono-dispersed. After using mixed chloroform/methanol solvent precipitation approach to narrow the size distribution, the gold nanoparticles finally obtained were dissolved in toluene to form a black colloidal solution. When evaporating a drop of the solution on a carbon-coated copper grid, we found a long-range-ordered hexagonal close-packed structure with a average space of about 1 nm between the about 2 nm sized nanoparticles, as shown in figure 6(a). The distance is far less than the twofold chain length of the 1-nonanethiol molecule, suggesting the interdigitation of the monolayer organic molecules adsorbed on the surface of the nanoparticles with each other. In terms of the 'soft sphere' model proposed by Korgel *et al* [15], we roughly estimate the interaction energy between two nanoparticles, which gives the attraction energy of about $kT \approx 26$ meV ($T = 298$ K), clearly indicating that the structure can stably exist under room-temperature conditions. However, it is worth noting that when

the energy provided by the environment increases to some extent, the 2D ordered structure can be easily destroyed. In figure 6(b), we find that necks have been formed between nanoparticles at some places and nanoparticles have become connected with each other under electron irradiation. Iijima and Ishihashi [16] reported that the shape of a single bare gold particle changed continually, through internal transforms, from a single crystal to a twinned crystal by irradiation by an electron beam, and it took place abruptly in less than 0.1 s. However, in our case the fusion of adjacent thiol-capped nanoparticles can be distinctly seen, as shown in figure 6(b). The structure change occurred in 1 s when the electron beam was focused into the ordered region. We believe that the change involves two processes, evaporation of the attached ligands and fusion of the bare nanoparticles through rapid movement. The irradiation by the electron beam provides the energy necessary for the escape of the thiol molecules from the nanoparticle surfaces. However, for a superlattice composed of larger gold nanoparticles (5–6 nm), even if irradiated for a long time, the disintegration of the ordered structure has not yet been found [17]. It appears that the latter configuration has higher stability than that of the smaller gold nanoparticles. The observations suggest that the larger nanoparticles provide greater opportunity for heat dissipation, and thereby avoid structural ruin.

4. Summary

1-Nonanethiol-protected 2 nm Au nanoparticles have been synthesized using a wet chemical method. The size distribution of the thus-obtained material was narrowed and was characterized using various techniques. The FT-IR and XPS results confirm that the black waxy powder is composed of nanoparticles consisting of a Au core and a 1-nonanethiol 3D SAM. UV–vis and XRD measurements demonstrate that the size of the nanoparticles is in quantum dot range. TEM measurements show the formation of a 2D ordered hexagonal close-packed structure, and further indicate that the structural stability can be effected by thermal irradiation from outside, which might have great benefits for the design of high-density integrated circuits in the light of suitable considerations of thermal dissipation.

Acknowledgment

This work was supported by a grant from the National Science Foundation.

References

[1] Schmid G 1994 *Clusters and Colloidal: From Theory to Application* (New York: VCH)
[2] Hostetler M J, Templeton A C and Murray R W 1999 *Langmiur* **15** 3782
[3] Weisbecker C S, Merritt M V and Whitesides G M 1996 *Langmiur* **12** 3763
[4] Andres R P, Bielefeld J D, Henderson J I, Janes D B, Kolagunta V R, Kubiak C P, Mahoney W J and Osifchin R G 1996 *Science* **273** 169
[5] Fitzmaurice D, Rao S N, Preece J A, Stoddart J F, Wenger S and Zaccheroni N 1999 *Angew. Chem. Int. Ed. Engl.* **38** 1147
[6] Boal K, IIhan F, DeRouchey J E, Thurn-Albrecht T, Russell T P and Rotello V M 2000 *Nature* **404** 746
[7] Brust M, Walker M, Bethell D, Schiffrin D J and Whyman R J 1994 *Chem. Soc. Chem. Commun.* 801
[8] Leff D V, Ohara P C, Heath J R and Gelbart W M 1995 *J. Phys. Chem.* **99** 7036
[9] Keily J, Fink J, Brust M, Bethell D and Schiffrin D J 1998 *Nature* **396** 444
[10] Sandhyarani N *et al* 2000 *Chem. Mater.* **12** 104
[11] Martin J E, Wilcoxon J P, Odinek J and Provencio P 2000 *J. Phys. Chem.* B **104** 9475
[12] Alzarez M M, Khoury J T, Schaaff T G, Shafigullin M N, Vezmar I and Whetten R L 1997 *J. Phys. Chem.* B **101** 3706
[13] Warren E 1990 *X-ray Diffraction* (New York: Dover) ch 13
[14] Chen S, Templeton A C and Murray R W 2000 *Langmiur* **16** 3543
[15] Korgel B A, Fullam S, Connolly S and Fitzmaurice D 1998 *J. Phys. Chem.* B **102** 8379
[16] Iijima S and Ichihashi T 1986 *Phys. Rev. Lett.* **56** 616
[17] Jiang P, Xie S S, Yao J N, He S T, Lin X, Zhang H X, Shi D X, Pang S J and Gao H J unpublished